Available online at www.sciencedirect.com
ScienceDirect
Journal of Molecular Catalysis A: Chemical 285 (2008) 48–57
JOURNAL OF MOLECULAR CATALYSIS A: CHEMICAL
www.elsevier.com/locate/molcata

FTIR study of the selective catalytic reduction of NO_2 with ammonia on nanocrystalline NaY and CuY

Sherrie Elzey [a], Anamika Mubayi [b], Sarah C. Larsen [b,*], Vicki H. Grassian [a,b,**]

[a] *Department of Chemical and Biochemical Engineering, University of Iowa, Iowa City, IA 52242, USA*
[b] *Department of Chemistry, University of Iowa, Iowa City, IA 52242, USA*

Received 15 November 2007; accepted 28 December 2007
Available online 19 January 2008

Abstract

In this study, the selective catalytic reduction (SCR) of NO_2 to N_2 and O_2 with ammonia at 298 K on nanocrystalline NaY, Aldrich NaY and nanocrystalline CuY was investigated using in situ Fourier transform infrared (FTIR) spectroscopy. It was determined that the kinetics of SCR were 30% faster on nanocrystalline NaY compared to Aldrich NaY. The superior performance of the nanocrystalline zeolite was attributed to an increase in external surface reactivity. External surface sites, which include silanol groups and extra framework alumina (EFAL), gave rise to differences in the adsorption of NO_2 and NH_3 on nanocrystalline NaY compared to commercial NaY. Copper cation-exchanged nanocrystalline Y resulted in an additional increase in the rate of SCR as well as distinct NO_2 and NH_3 adsorption sites associated with the copper cation. This is the first study of a transition metal cation-exchanged nanocrystalline zeolite and its potential use as a catalyst in the SCR of nitrogen oxides.

Keywords: Selective catalytic reduction; Ammonia; Zeolite Y; Nanocrystalline

1. Introduction

Emissions of NO_x ($NO + NO_2$) are generated during combustion processes and adversely affect the environment and human health by contributing to ground-level ozone formation, water quality deterioration, global warming, production of toxic reaction products and inhalable fine particles that lead to visibility degradation and pose a respiratory hazard. The primary sources of NO_x emissions include motor vehicles (55%) and industrial, commercial, and residential combustion processes (45%). Current NO_x reduction technology uses catalysts to convert NO_x to environmentally benign products, such as N_2, O_2 and H_2O, during reaction with a reductant through the process of selective catalytic reduction (SCR). NO_x emissions remain in excess of Environmental Protection Agency (EPA) emission limits, and catalysts that improve NO_x reduction are necessary to tackle this problem.

Metal oxides have commonly been used as catalysts for SCR of NO_x, but zeolites have been shown to have superior activity due to their ability to achieve higher NO_x conversions at lower temperatures [1]. Zeolites are crystalline aluminosilicates, consisting of regularly occurring internal pores of molecular dimensions, and a framework of linked cages or channels. The porous nature of zeolites has led to a wide variety of applications based on adsorption/desorption, ion exchange, and catalysis. Many studies have focused on ZSM-5 zeolites for deNO_x applications, but, despite the superior activity of ZSM-5 zeolites, results have shown problematic deactivation occurs under typical combustion conditions where water and oxygen are present [2]. Zeolite Y has a different channel structure that could provide unique SCR pathways and may offer a more practical choice of catalyst for post-combustion NO_x treatment. Zeolite Y has a three-dimensional pore structure consisting of sodalite cages with a 7.4 Å diameter assembled to form larger supercages with a 1.2 nm diameter [3]. The framework carries a net negative charge, and charge-compensating metal cations can reside within the interior of the framework and on the exterior as extra framework cations.

Metal cations associated with the zeolite framework are loosely bound and can be easily exchanged. Such cation

* Corresponding author. Tel.: +1 319 335 1346; fax: +1 319 335 1270.
** Corresponding author. Tel.: +1 319 335 1392; fax: +1 319 335 1270.
E-mail addresses: sarah-larsen@uiowa.edu (S.C. Larsen), vicki-grassian@uiowa.edu (V.H. Grassian).

1381-1169/$ – see front matter © 2008 Elsevier B.V. All rights reserved.
doi:10.1016/j.molcata.2007.12.032

exchange can influence the activity of zeolites, and the effect of transition metal cation exchange on the activity of zeolite Y for SCR of NO_x has been thoroughly studied [4–6]. Polyvalent cations were shown to enhance activity compared with monovalent cations, and copper cation exchange resulted in the highest activity. Sachtler et al. suggested that the multipositive charge of polyvalent cations can dissipate due to dissociative adsorbates such as H_2O and N_2O_4, allowing the cation to migrate toward localized negative charges, thus lowering the energy of the system [1]. Such energetically favorable dissociation could improve the activity of CuY for SCR of NO_2, as NO_2 is known to form dimers that dissociate during adsorption on zeolite Y as

$$2NO_2 \rightarrow N_2O_4 \quad (1)$$

$$N_2O_4 \rightarrow NO_3^- + NO^+ \quad (2)$$

Due to the increased activity of copper-exchanged zeolites, and the large copper ion exchange capacity of zeolite Y compared with other zeolites, several studies have investigated the copper cation interaction with the zeolite Y framework [6–11]. Selyama et al. identified sites occupied by Cu(II) cations within the framework of zeolite Y and determined that there were five unique sites of Cu(II) cations within the sodalite and supercage of zeolite Y [7]. The sodalite cage sites were much more densely populated than the supercage sites, but adsorbed water and ammonia can coordinate with the copper cations and cause migration from the sodalite cages to the supercage. Such migration upon water or ammonia adsorption and enhanced mobility of copper ions in CuY has also been reported by others [6,8]. The catalytic activity of CuY for SCR of NO_x has shown a unique temperature dependence with maximum activity occurring at 393 K. The coordination of ammonia with Cu(II) to form a $[Cu(NH_3)_4]^{2+}$ complex, accompanied by migration to the supercage, was suggested to be the cause of the unusual temperature dependency [6]. At increased temperatures, ammonia molecules desorb, causing migration back to the sodalite cages and a decrease in activity. In contrast to studies suggesting SCR occurs in the presence of coordinated Cu(II), a kinetic study of NH_3-SCR of NO over CuY suggested a three-step mechanism based on an Eley-Rideal interaction where one ammonia molecule is initially bound to Cu(I) [12]. In this mechanism, Cu(I) is oxidized to Cu(II)N_xO_y by oxygen then by NO, and the ammonia reacts with the N_xO_y on the same cation to produce N_2 and H_2O and regenerate the initial NH_3Cu(I).

In addition to the effect of metal cation exchange on deNO_x performance, the effect of particle size of zeolites as catalysts for deNO_x applications has recently been considered [13–15]. Commercial zeolites have particle sizes ranging from several hundred nanometers to over a micron. Nanocrystalline zeolites with particle sizes less than 100 nm have been synthesized and possess unique properties compared with commercial zeolites, including greater total and external surface area, a larger percentage of total surface area as external surface area, decreased diffusion pathlengths, and an increased concentration of reactive sites [13].

Most relevant to the work in this paper are previous studies comparing nanocrystalline NaY with commercial Aldrich NaY for propylene-SCR of NO_2 and urea-SCR of NO_2 [14,15]. Nanocrystalline NaY zeolite with a particle size of 23 nm was shown to be superior to Aldrich NaY with a particle size of over 500 nm for both propylene-SCR and urea-SCR of NO_2 due to faster reaction rates and decreased formation of undesirable products. The superior performance of the smaller particle sized nanocrystalline NaY was attributed to increased external surface area, silanol groups found in greater concentration on nanocrystalline zeolites, and extra framework alumina (EFAL) sites with Brønsted and Lewis acidity identified on the external surface of the nanocrystalline NaY.

The mechanisms, thermodynamic dependencies and kinetics of the reactions involved in NH_3-SCR of NO_x using commercial zeolites have been investigated in a number of studies [16–22]. In this study, Aldrich NaY, nanocrystalline NaY and nanocrystalline CuY were evaluated for NH_3-SCR of NO_2. A comparison of surface species before and after SCR, as well as intermediates and product formation, for Aldrich NaY, nanocrystalline NaY, and nanocrystalline CuY is presented. Results for reaction rates and temperature studies are also discussed.

2. Experimental methods

2.1. Synthesis and copper exchange of nanocrystalline NaY

The synthesis of nanocrystalline NaY has been described previously [23,24]. The original synthesis gel composition for zeolite Y was

$$0.07Na : 2.4TMAOH : 1.0Al : 2.0Si : 132H_2O : 3.0i\text{-}PrOH : 8.0EtOH$$

where TMAOH is tetramethylammonium hydroxide. Aluminumisopropoxide and tetraethylorthosilicate (TEOS) were used as aluminum and silicon sources, respectively, with isopropanol (*i*-PrOH) and ethanol (EtOH) as their respective hydrolysis products. The synthesis solution for zeolite Y was heated to 363 K in a glass flask containing a magnetic stirrer for 240 h for the first batch, and 72 h for later batches. After each batch, the zeolite crystals were recovered by centrifugation at 14,000 rpm for 30 min. After washing and drying, X-ray powder patterns and BET surface areas of the powders were measured to determine crystal structures and crystal sizes. The NaY was then calcined at 773 K under oxygen flow for 16 h to remove the TMAOH template. The sodium in nanocrystalline NaY was exchanged with copper ions using the vapor phase exchange method [23]. Approximately 250 mg of synthesized, calcined nanocrystalline NaY and 25 mg of dry copper(I) chloride were ground together using a mortar and pestle. The solid mixture was placed in a glass tube and evacuated for 3 h at room temperature and then heated under vacuum at 673 K for 6 h.

2.2. Characterization of zeolites

The synthesized nanocrystalline NaY and CuY, as well as commercial NaY purchased from Aldrich, were characterized using the following techniques.

2.2.1. Elemental analysis

A PerkinElmer Plasma 400 Inductively Coupled Plasma Atomic Emission Spectrometer (ICP/AES) spectrometer was used to determine the Si/Al ratio of the NaY samples. NaY samples were acid digested by dilute HF solution followed by neutralization in $NaBO_3$. Four standard solutions with known silicon (aluminum, sodium, and copper) concentrations were prepared as calibration standards. Exact concentrations of silicon, aluminum, sodium and copper in the sample solution were obtained by projection from the working curve generated from standard solution data.

2.2.2. Hitachi S-4800 scanning electron microscope

SEM samples were prepared by sonicating the calcined zeolite powder in a dilute methanol suspension to break up particle agglomerates. A drop of the suspension was applied to the SEM sample stud, and the methanol was allowed to evaporate at room temperature. The sample was then coated with gold, and SEM images were acquired.

2.2.3. X-ray diffraction (XRD)

A Siemens D5000 X-ray diffractometer with Cu Kα target and nickel filter was used to collect XRD powder patterns for the samples. XRD patterns were collected between 2θ angles of 5° and 35°.

2.2.4. Electron paramagnetic resonance

Continuous wave electron paramagnetic resonance (EPR) spectra were acquired using a Bruker EMX61 EPR spectrometer equipped with a PC for spectrometer control and data acquisition. Typical EPR spectral parameters were X-band frequency = 9.43 GHz, modulation amplitude = 0.5 G and modulation frequency = 100 kHz. The magnetic field and microwave frequency were measured using a Hall probe and a frequency counter, respectively.

2.2.5. Nitrogen adsorption isotherms

Nitrogen adsorption isotherms were collected using a Quantachrome Nova 4200e multipoint BET apparatus. Approximately 0.1–0.2 g of each sample was used for the measurements. Samples were heated at 533 K and degassed overnight prior to nitrogen adsorption. The specific surface area of each sample was then measured. BET adsorption isotherms were collected for nanocrystalline NaY samples before and after calcination to remove the template.

2.3. FTIR experiments

Zeolite samples (10–15 mg) were sonicated in methanol for 30 min at room temperature to produce a hydrosol. For the nanocrystalline samples, the powder was crushed with a mortar and pestle to break up agglomerates prior to sonication. The hydrosol was then transferred by pipette to one half of a tungsten grid, and the methanol evaporated at room temperature to create a uniform thin film. A thermocouple wire was attached to the tungsten grid to allow resistive heating. The sample holder was placed in a stainless steel reaction chamber equipped with a linear translator to allow either the gas phase or the zeolite sample to be placed in the path of the FTIR beam. The reaction chamber was connected to a power supply and vacuum/gas handling system. Details of the FTIR experimental system have been described previously [25].

WinFirst software was used to acquire the data, and spectra were recorded using 64 averaged scans with a resolution of 4 cm^{-1}. Gas phase spectra were referenced to the blank grid, and absorbance spectra were referenced to the corresponding gas phase background with the clean zeolite subtracted. Zeolite samples were heated overnight at 600 K under vacuum prior to experiments. The sample was allowed to cool to room temperature before gases were admitted into the reaction chamber. For absorbance spectra of the surface species resulting from adsorption of reactant gases (NO_2 and NH_3), the gas was loaded into the reaction chamber and the pressure was allowed to stabilize to ensure adsorption equilibrium. The gas phase was then pumped out prior to collecting the spectra. For SCR experiments, 1.5 Torr of NO_2 was loaded into the reaction chamber. Upon equilibration of the NO_2, 1.5 Torr NH_3 was loaded into the reaction chamber, and heat was applied for experiments conducted at elevated temperatures. For time course experiments, FTIR spectra of the gas phase were automatically collected every 30 s for 2 h. All spectra shown were recorded at 298 K.

Concentrations of species present in the gas phase were obtained by multiplying the integrated absorbance of the characteristic absorption bands by a correlation factor based on the extinction coefficient of each species. The extinction coefficients were calibrated using the integrated absorbance of the characteristic bands at corresponding pressures measured with an absolute pressure transducer [15]. Changes in NO_2 concentration with reaction time were used to determine initial reaction rates for each zeolite sample at various reaction temperatures.

3. Results

3.1. Characterization of zeolites

SEM images of nanocrystalline NaY and Aldrich NaY are shown in Fig. 1. The image of Aldrich NaY (Fig. 1B) shows large crystals and a wide range of particle sizes, with diameters of ∼0.5–1.5 μm, and an average particle diameter estimated to be ∼1 μm. The image of nanocrystalline NaY (Fig. 1A) shows uniform particles with a narrow size range and an average diameter of approximately 38 nm. The particle size, surface area and catalyst composition for the three zeolite samples are given in Table 1. The total specific surface area of calcined NaY was measured using nitrogen adsorption and the BET method. The external surface area was determined using the BET method for as-synthesized zeolites, which still have template blocking the pores and was used to calculate crystal size [3]. Two different batches of nanocrystalline NaY were used in this study but the crystal sizes were similar, 38 and 34 nm, as determined from the external surface area. The external surface areas of the nanocrystalline NaY samples were >100 m^2/g, representing ∼20% of the total surface area.

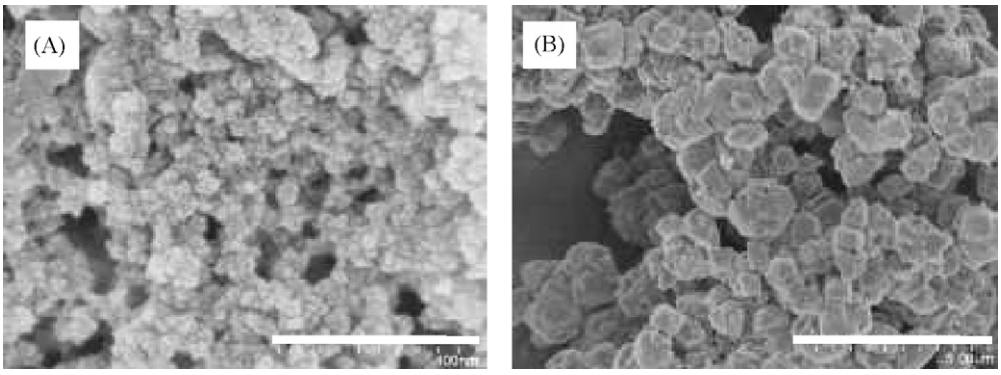

Fig. 1. SEM images of NaY: (A) nanocrystalline NaY (scale bar = 400 nm) and (B) Aldrich NaY (scale bar = 5 μm).

The samples were characterized by powder X-ray diffraction and electron paramagnetic resonance spectroscopy. XRD powder patterns of the NaY samples (Fig. 2) were obtained before and after vapor phase exchange. Broadening of the XRD pattern is observed for nanocrystalline NaY relative to Aldrich NaY and this is due to the expected line broadening that occurs as the crystal size becomes very small. The crystal structure is intact after the vapor phase exchange as indicated by the XRD pattern in Fig. 2c.

Table 1
Properties of synthesized nanocrystalline NaY and CuY and Aldrich NaY

Zeolite catalyst	Particle size (nm)	Total/external specific surface area (m^2/g)	Si/Al	Cu/Al
Aldrich NaY	~1000	615/<1[a]	1.8	–
Nano-NaY	38[b]	523/106	1.8	–
Nano-CuY	34[b]	538/118	1.8	0.3

[a] Estimated based on geometric considerations.
[b] Determined from BET external surface area measurements as in Ref. [3].

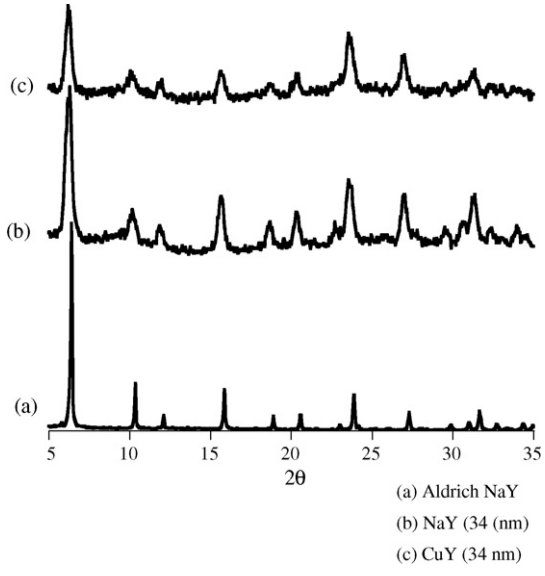

Fig. 2. XRD patterns of synthesized nanocrystalline NaY and CuY and Aldrich NaY.

The EPR spectrum was obtained for nanocrystalline CuY at 77 K and is shown in Fig. 3. Cu(II) has a d^9 electronic configuration with $S = 1/2$ and $I = 3/2$. The EPR spectrum of nanocrystalline CuY has the same general features as hydrated, octahedral $[Cu(H_2O)_6]^{2+}$ or $[Cu(H_2O)_5OH]^{+}$ complexes, but the spectral broadening makes it difficult to quantitatively determine the EPR parameters through simulation or fitting routines [26,27]. The spectral broadening is attributed to the heterogeneity of the copper sites in the nanocrystalline CuY.

3.2. Adsorption of NO_2 at $T = 298$ K

The FTIR spectra of Aldrich NaY, nanocrystalline NaY and nanocrystalline CuY with adsorbed NO_2 are shown in Fig. 4. The assignment of absorption bands resulting from NO_2 adsorption on all three zeolites is summarized in Table 2. Absorption bands appear at 1212, 1308, 1395, and 2180 cm^{-1} upon NO_2 adsorption on Aldrich NaY. The assignment of these bands is based on comparison with previous literature [15,18,19,22]. The band at 1212 cm^{-1} is due to nitrite adsorbed on sodium cationic sites, and the band at 1395 cm^{-1} and its shoulder at 1308 cm^{-1} are due to nitrate adsorbed on sodium cationic sites. The two nitrate bands result from splitting of the degenerate asymmetric stretching vibration and broaden into one band at higher NO_2 loadings. The broadening is due in part to intermolecular inter-

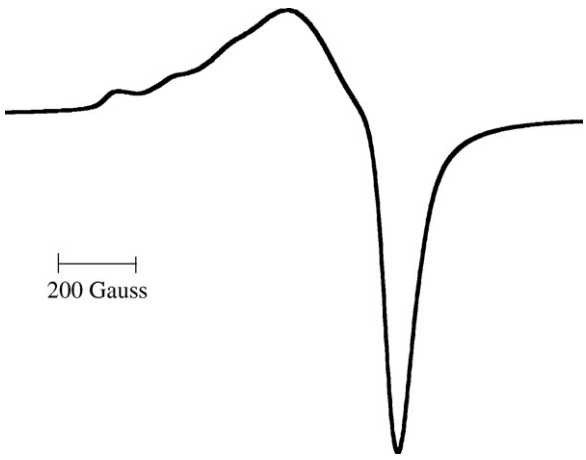

Fig. 3. EPR spectrum of nanocrystalline CuY recorded at 77 K.

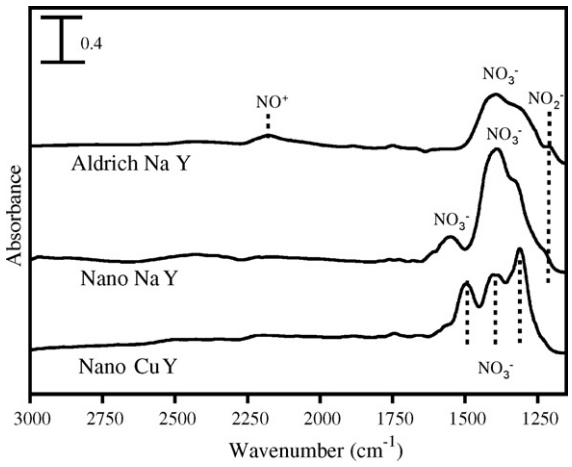

Fig. 4. FTIR spectra of NO_2 adsorbed on Aldrich NaY, nanocrystalline NaY and nanocrystalline CuY at $T = 298$ K. A pressure of 1.5 Torr NO_2 was allowed to equilibrate, and the gas phase was pumped out prior to collecting each spectrum. The blank grid was used as a reference, and the corresponding clean zeolite spectrum prior to NO_2 adsorption has been subtracted.

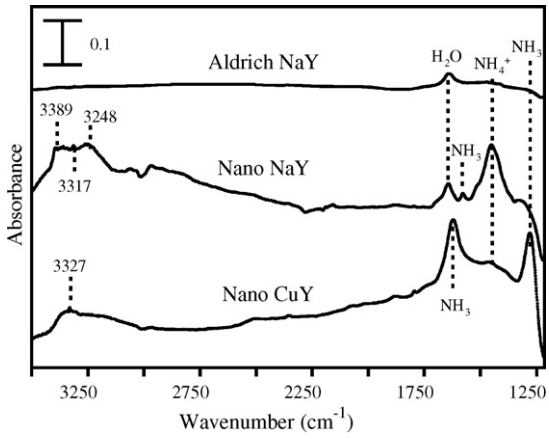

Fig. 5. FTIR spectra of NH_3 adsorbed on Aldrich NaY, nanocrystalline NaY and nanocrystalline CuY at $T = 298$ K. The gas phase was pumped out prior to collecting each spectrum. The blank grid was used as a reference, and the corresponding clean zeolite spectrum prior to NH_3 adsorption has been subtracted.

actions [25]. The band at 2180 cm^{-1} resulted from the formation of $[NO^+][NO_2]$ adducts on Lewis base sites [14].

Absorption bands on nanocrystalline NaY following exposure to NO_2 appear at 1226, 1326, 1394, and 1555 cm^{-1}. These bands are easily assigned based on previous studies of urea-SCR of NO_2 over nanocrystalline NaY [15]. Similar to Aldrich NaY, NO_2 adsorption on nanocrystalline NaY resulted in adsorbed nitrite (1226 cm^{-1}) and nitrate (1326 and 1394 cm^{-1}) on sodium cationic sites. The band at 1555 cm^{-1} is due to nitrate adsorbed on EFAL sites in a monodentate coordination, and is only observed in the nanocrystalline NaY. The intensity of the nitrate bands in nanocrystalline NaY relative to Aldrich NaY indicate the greater adsorption capacity of nanocrystalline NaY for NO_2. Formation of NO^+ evidenced by a band at ~2080 cm^{-1} is weak on nanocrystalline NaY. This is most likely due to increased surface reactive sites in nanocrystalline NaY that allow NO_2 to adsorb as surface nitrate without the production of NO^+, or promote the conversion of NO^+ to surface nitrite:

$$O_{(surface)}{}^- + NO_2 \rightarrow NO_3{}^- \quad (3)$$

$$NO^+ + O_{(surface)}{}^{2-} \rightarrow NO_2{}^- \quad (4)$$

Table 2
Assignment of absorbance bands resulting from NO_2 adsorption on Aldrich NaY, nanocrystalline NaY and nanocrystalline CuY

Catalyst	Frequency (cm^{-1})	Assignment of adsorbed species	Reference
Aldrich NaY	1212	$\nu(NO_2{}^-)$ of $NO_2{}^-$ ads on Na^+	
	1308, 1395	$\nu(NO_3{}^-)$ of $NO_3{}^-$ ads on Na^+	[25]
	2180	$\nu(NO^+)$ of $[NO^+][NO_2]$ on Na^+	[14]
Nano-NaY	1226	$\nu(NO_2{}^-)$ of $NO_2{}^-$ ads on Na^+	
	1326, 1394	$\nu(NO_3{}^-)$ of $NO_3{}^-$ ads on Na^+	[15]
	1555	$\nu(NO_3{}^-)$ of $NO_3{}^-$ on EFAL	
Nano-CuY	1313, 1397, 1498	$\nu(NO_3{}^-)$ of $NO_3{}^-$ ads on Cu^{2+}	[28]

Absorption bands for the nanocrystalline CuY appear at 1313, 1397, and 1498 cm^{-1}. The three bands overlap and fall within the nitrate adsorption range observed for both NaY zeolites. These bands are assigned to nitrate adsorbed on copper cationic sites, and the nature of these surface species has been discussed previously [28]. A shoulder at higher wavenumber above 1500 cm^{-1} is observed, most likely due to nitrate adsorbed on EFAL sites, as observed in nanocrystalline NaY.

3.3. Adsorption of NH_3 at $T = 298$ K

FTIR spectra of Aldrich NaY, nanocrystalline NaY and nanocrystalline CuY with adsorbed NH_3 are shown in Fig. 5. The assignment of absorption bands resulting from NH_3 adsorption on all three zeolites is summarized in Table 3. The presence of

Table 3
Assignment of absorbance bands resulting from NH_3 adsorption on Aldrich NaY, nanocrystalline NaY and nanocrystalline CuY

Catalyst	Frequency (cm^{-1})	Assignment of adsorbed species	Reference
Aldrich NaY	1311	$\delta(NH_3)$ of NH_3 on SiOH	[22,30,31]
	1475	$\delta(NH_4{}^+)$ of $NH_4{}^+$ deformation	
	1641	$\delta(H_2O)$ of adsorbed H_2O	
Nano-NaY	1308	$\delta(NH_3)$ of NH_3 on SiOH	
	1450	$\delta(NH_4{}^+)$ of $NH_4{}^+$ deformation	
	1580	$\delta(NH_3)$ of NH_3 on EFAL	[29]
	1641	$\delta(H_2O)$ of adsorbed H_2O	
	3248	$\nu(NH_3)$ of NH_3 on O^{2-} of SiOH	
	3317	$\nu(NH_3)$ sym. stretch of NH_3 on surface OH	[22,30,31]
	3389	$\nu(NH_3)$ asym. stretch of NH_3 on surface OH	
Nano-CuY	1282	$\delta(NH_3)$ of NH_3 in $[Cu(NH_3)_4]^{2+}$	[10]
	1460	$\delta(NH_4{}^+)$ of $NH_4{}^+$ deformation	
	1623	$\delta(NH_3)$ of NH_3 in $[Cu(NH_3)_4]^{2+}$	

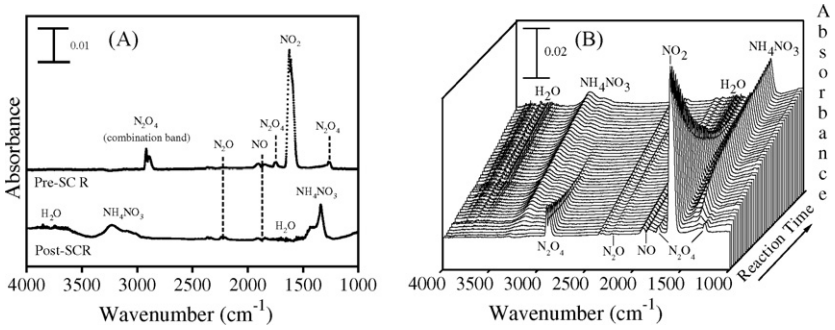

Fig. 6. FTIR spectra of gas phase species detected (A) pre-SCR and post-SCR over nanocrystalline CuY at $T = 298$ K, and (B) at 30 s intervals for the first 30 min during SCR over nanocrystalline CuY at $T = 298$ K. The blank grid was used as a reference.

NH_3 resulted in absorption bands due to molecularly adsorbed ammonia and the formation of ammonium ions in all three zeolites. For nanocrystalline NaY, absorption bands are observed at 1308, 1450, 1580, 1641, 3248, 3317, and 3389 cm^{-1}. The broad band at 1308 cm^{-1} is assigned to NH_3 adsorbed on Lewis acid sites, the intense band at 1450 cm^{-1} is assigned to NH_4^+ resulting from ammonia protonation by Brønsted acid sites, the small peak at 1580 cm^{-1} is assigned to NH_3 adsorbed on EFAL sites, and the peak at 1641 cm^{-1} is due to adsorbed water [29]. The band at 3248 cm^{-1} is likely due to ammonia hydrogen bonded to oxygen lone pairs of silicon–oxygen bridging sites [30,31]. The bands at 3317 and 3389 cm^{-1} are the symmetric and asymmetric stretches of ammonia adsorbed on surface hydroxyl groups [22,30,31].

Aldrich NaY showed absorption bands at 1311 and 1475 cm^{-1} due to NH_3 on Lewis acid sites and NH_4^+ formation, respectively, but these bands were much weaker than those on the nanocrystalline sample. Additionally, there was no band resulting from NH_3 on EFAL sites for the Aldrich NaY. The greater intensity of the bands on the nanocrystalline NaY and the observation of NH_3 on EFAL sites are due to the increased concentration of surface reactive sites present in the nanocrystalline zeolite. The small, sharp band commonly reported by others at ~1620–1630 cm^{-1} due to NH_3 adsorbed on Lewis acid sites of NaY was not observed on the Aldrich or nanocrystalline NaY samples [32,33]. This band could have been dominated by absorption due to water on both NaY samples.

There were differences in ammonia adsorption between the nanocrystalline samples. Absorbance bands on the nanocrystalline CuY are seen at 1282, 1460, 1623, and 3327 cm^{-1}. The broad band at 1460 cm^{-1} is due to NH_4^+ formation, and the sharper bands at 1282 and 1623 cm^{-1} are assigned to NH_3 coordination with copper cations, resulting in a $[Cu(NH_3)_4]^{2+}$ complex [10]. The NH_4^+ band on the nanocrystalline CuY is weaker, and the NH_3 bands are more intense relative to the nanocrystalline NaY. This is due to the fact that ammonia formed strong coordination bonds with the copper cations, leaving fewer NH_3 molecules for protonation and NH_4^+ formation. The band at 3327 cm^{-1} is most likely the symmetric stretch of ammonia adsorbed on surface hydroxyl groups.

3.4. NH_3-SCR of NO_2 at $T = 298$ K: gas phase

A gas phase spectrum was collected prior to running the SCR reaction, with only NO_2 loaded in the reaction chamber. As described earlier, ammonia was added to begin the SCR, and the gas phase was monitored at 30 s intervals for the duration of the reaction. A final gas phase spectrum was collected after two hours of SCR. Results for nanocrystalline CuY before, during, and after SCR are shown in Fig. 6. The nanocrystalline CuY gas phase spectra are representative of all three zeolite samples, since both NaY zeolites showed similar product formation compared to CuY. Prior to SCR, gas phase species present were NO_2, N_2O_4, NO (~1:3 ratio NO:NO_2) and a small amount of N_2O (~1:100 NO:NO_2). After two hours of NH_3-SCR at 298 K the peaks due to NO_2 and N_2O_4 completely disappeared, and small bands due to NO and N_2O still remained. Water was produced, and an ammonium nitrate intermediate was seen in the gas phase due to condensation on the IR cell windows. The absorption bands for ammonium nitrate remained in the IR spectrum after pumping out the gas phase and slowly disappeared with continued evacuation of the IR cell. This suggests ammonium nitrate was condensed on the IR cell windows rather than present in the gas phase. Nitrogen was also produced during SCR according to the overall equation for NH_3-SCR of NO_2:

$$2NH_3 + 2NO_2 \rightarrow NH_4NO_3 + N_2 + H_2O \quad (5)$$

Gas phase NO and N_2O remain after SCR of NO_2. These species are greenhouse gases, and can either be produced during SCR or be present prior to SCR in the NO_2 gas feed and remain unreacted. The gas phase concentrations of NO and N_2O during NH_3-SCR of NO_2 are shown in Fig. 7. All three zeolite samples showed similar results for both NO and N_2O in the gas phase. The total concentration of gas phase NO was reduced by ~30–40% during the SCR reaction. It could be expected that under typical lean burn exhaust conditions a greater amount of NO would be oxidized to NO_2 according to

$$NO + (1/2)O_2 \rightarrow NO_2 \quad (6)$$

and subsequently reduced during NH_3-SCR of NO_2.

In the presence of oxygen, N_2O can be produced from reactions with ammonia and NO. In the presence or absence of

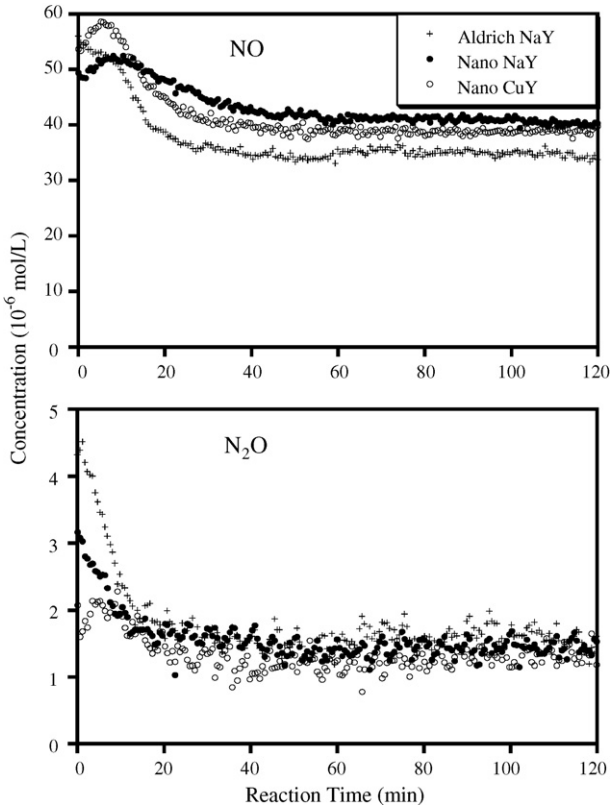

Fig. 7. Concentrations of gas phase NO (upper) and N_2O (lower) over Aldrich NaY, nanocrystalline NaY and nanocrystalline CuY as a function of time during NH_3-SCR of NO_2 at $T = 298$ K.

oxygen, N_2O can also be produced from the thermal degradation of ammonium nitrate:

$$NH_4NO_3 \rightarrow N_2O + 2H_2O \quad (7)$$

The results of this research show no production of N_2O during SCR under these reaction conditions. There was initially a small concentration of N_2O, which decreased during the course of the reaction. Although ammonium nitrate was present, degradation producing N_2O did not occur since the ammonium nitrate remained in a condensed state due to the relatively low temperature of the reaction.

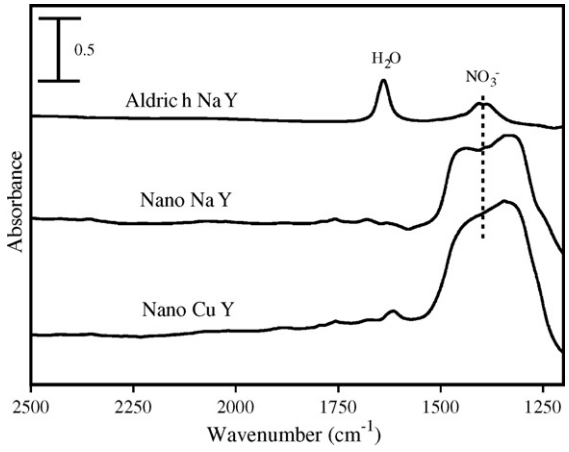

Fig. 8. FTIR spectra of surface species detected post-SCR over Aldrich NaY, nanocrystalline NaY and nanocrystalline CuY at $T = 298$ K. The gas phase was pumped out prior to collecting each spectrum, and the blank grid was used as a reference. Corresponding clean zeolite spectra prior to SCR have been subtracted.

3.5. NH_3-SCR of NO_2 at $T = 298$ K: surface species

Prior to SCR, surface species observed on the zeolites were due to NO_2 adsorption only, which has been described previously (Fig. 4). Results for the surface species detected post-SCR over Aldrich NaY, nanocrystalline NaY and nanocrystalline CuY are shown in Fig. 8. All three zeolite samples showed NO_3^- remaining on the surface due to adsorption on cationic sites. Aldrich NaY had water remaining on the surface at 1638 cm^{-1} and nitrate at 1410 cm^{-1}. As mentioned earlier, two nitrate bands on NaY have been known to merge at higher NO_2 concentrations. Nitrate is seen as a merging of the two bands on the surface of nanocrystalline NaY post-SCR, with two maxima at 1335 and 1440 cm^{-1}. Nitrate adsorbed on EFAL sites in nanocrystalline NaY was more reactive than nitrate on cationic sites since no nitrate remained on EFAL sites post-SCR. For nanocrystalline CuY post-SCR, NO_3^- is seen as a very broad band. Comparing the shape and location of this band with the three nitrate bands seen on CuY pre-SCR (Fig. 4) suggests the nitrate band post-SCR resulted from an overlapping of the three nitrate bands seen pre-SCR. The intensity of the nitrate band on Aldrich NaY is significantly lower than on nanocrystalline NaY, and nanocrystalline CuY has an even more intense nitrate band. The small peak at 1617 cm^{-1} on nanocrystalline CuY is most likely due to a small amount of adsorbed NH_3 remaining post-SCR [34].

3.6. Nanocrystalline zeolites: NaY versus CuY

A primary aim of this work was to compare nanocrystalline zeolites with sodium and copper cations for NH_3-SCR of NO_2. It is well known that copper cation exchange improves the performance of commercial zeolites for deNO_x applications, as determined by higher NO_x conversions, faster reaction rates and lower temperatures required for SCR [1,4–6]. Not surprisingly, similar results were observed for nanocrystalline zeolites. The concentration of NO_2 present in the gas phase during SCR over Aldrich NaY, nanocrystalline NaY and nanocrystalline CuY is shown in Fig. 9. The reaction kinetics for NO_2 loss appeared to be zero order, as indicated by the linear nature of the time-dependent NO_2 concentration. The reaction occurred very quickly over the nanocrystalline zeolites, with greater than 97% conversion achieved in less than 20 min. The initial rates of reaction for nanocrystalline NaY and CuY are compared in

Table 4
Comparison of initial rates of reactions for NH_3-SCR of NO_2 over Aldrich NaY, nanocrystalline NaY and nanocrystalline CuY

Zeolite catalyst	Initial rate ((mol L^{-1} min^{-1} mg^{-1})	% improvement over Aldrich NaY
Aldrich NaY	0.50	0
Nano-NaY	0.70	29
Nano-CuY	0.83	40

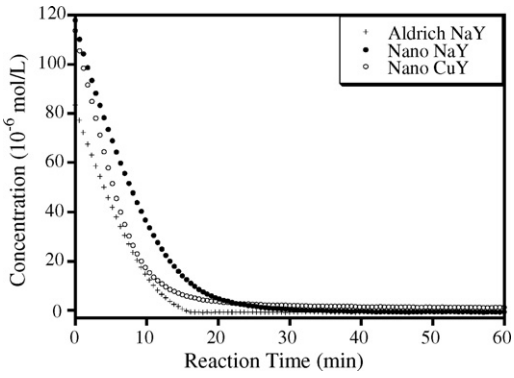

Fig. 9. Concentration of gas phase NO_2 over Aldrich NaY, nanocrystalline NaY and nanocrystalline CuY during NH_3-SCR of NO_2 at $T = 298$ K.

Table 4, along with Aldrich NaY. Nanocrystalline CuY showed an increased reaction rate of 11% compared with nanocrystalline NaY, and 40% compared to Aldrich NaY. The superior performance of nanocrystalline NaY over Aldrich NaY for NH_3-SCR of NO_2 is attributed to the enhanced properties of nanocrystalline zeolites compared with zeolites of larger particle size previously reported for SCR of NO_2 with propylene and urea as the reductants [14,15]. The superior performance of nanocrystalline CuY over nanocrystalline NaY requires an explanation that is independent of the nanocrystalline nature of the zeolite, but instead is specific to the identity of the cation present in the framework. This is discussed in further detail below in Section 4.

Temperature studies showed an interesting difference between the two nanocrystalline zeolites. SCR reactions were carried out at 298, 373, 423, and 473 K. Reaction rates for nanocrystalline NaY were independent of temperature, with less than 3% variation in the reaction rate at all four temperatures studied. Nanocrystalline CuY showed an inverse temperature dependence, with an average decrease in reaction rate of nearly 7% for each 50 K rise in temperature. This observation is related solely to the difference of the exchangeable cation, since the Aldrich NaY showed the same temperature dependence as the nanocrystalline NaY.

4. Discussion

4.1. NH_3-SCR of NO_2: reactions between NO_2 and NH_3

Ammonia can react with NO_x during SCR according to

$$4NH_3 + 4NO + O_2 \rightarrow 4N_2 + 6H_2O \quad (8)$$

$$2NH_3 + NO + NO_2 \rightarrow 2N_2 + 3H_2O \quad (9)$$

$$4NH_3 + 3NO_2 \rightarrow 3.5N_2 + 6H_2O \quad (10)$$

Typical combustion exhaust conditions contain ~16% water and an excess of oxygen, leading to numerous side reactions, including direct oxidation of ammonia to produce N_2, N_2O, NO_2, or NO, and oxidation of NO to NO_2 [16]. The reaction resulting from NH_3 and an equimolar mixture of NO and NO_2 (4) is said to be the fast SCR reaction, while mixtures containing greater fractions of NO_2 (5) are said to proceed more slowly. Common intermediates in NH_3-SCR of NO_x include ammonium nitrite and ammonium nitrate.

Selective catalytic reduction of NO_x with ammonia is defined by the formation of N_2 as the preferred product. It is widely accepted that the N_2 product contains one nitrogen atom originating from NO_x and one from NH_3 [2,15,21]. In this work, the production of N_2 during SCR could be a composite of reactions based on the surface and gas phase species observed. Reactions would then involve adsorbed ammonia (NH_3, NH_4^+) and/or gas phase NH_3 interacting with adsorbed NO_2 (NO_3^-, NO_2^-, and NO^+) and/or gas phase NO_2 (NO_2, N_2O_4, N_2O, and NO) (Figs. 4–6). Insight into the probable interactions between NO_2 and NH_3 for the three zeolites can be gained by considering the surface species formed upon adsorption of the reactants on each zeolite.

All three zeolites showed similar major surface species upon adsorption of both NO_2 and NH_3, but the reactive sites where adsorption occurred were different. The major surface species formed from NO_2 adsorption on Aldrich NaY was NO_3^- adsorbed on Na^+ sites. Minor surface species included NO_2^- and NO^+ on Na^+ sites. Ammonia resulted in a small amount of NH_3 adsorbed on silanol groups only. From the analysis of surface species formed upon reactant adsorption it is determined that SCR reactions between NO_2 and NH_3 over Aldrich NaY occurred primarily between nitrate on sodium cationic sites and NH_3 on silanol groups.

Similar to Aldrich NaY, the major surface species formed from NO_2 adsorption on nanocrystalline NaY was NO_3^- on Na^+ sites, and a minor surface species was NO_2^- on Na^+ sites. Unique to nanocrystalline NaY was NO_3^- adsorbed on EFAL sites as well. Nitrate adsorbed on EFAL sites was more reactive than nitrate on Na^+ sites since only nitrate on the Na^+ remained on the surface post-SCR. Also unique to nanocrystalline NaY was NH_3 adsorbed on EFAL sites in addition to NH_3 adsorbed on silanol groups. This indicates that SCR reactions between NO_2 and NH_3 over nanocrystalline NaY involved nitrate on sodium cationic sites *and* EFAL sites reacting with NH_3 on silanol groups *and* EFAL sites.

Adsorption of NO_2 and NH_3 on nanocrystalline CuY resulted in the same major surface species of NO_3^- and NH_3, respectively. An interesting difference was that all the surface species identified on nanocrystalline CuY for both NO_2 and NH_3 were adsorbed on copper cationic sites. A small amount of NO_2 was also suggested to result from adsorption on EFAL sites. Therefore, SCR reactions between NO_2 and NH_3 over nanocrystalline CuY were determined to have occurred between nitrate on copper cationic sites and EFAL sites and NH_3 on copper cationic sites. This result suggests that copper cation exchange not only resulted in faster NH_3-SCR of NO_2, but also indicates the copper cations played a greater role in facilitating the SCR than sodium cations, even dominating the Lewis and Brønsted acid sites primarily involved in SCR over zeolites.

The production of N_2 was initiated by NO_2 dimerization and subsequent dissociation to NO_3^- and NO^+, together with NO_2 and NO^+ interactions with surface oxygen anions to produce NO_3^- and NO_2^- according to reactions (3) and (4). This work indicates that these surface species reacted solely with

adsorbed NH_3 rather than gas phase NH_3, since gas phase NH_3 concentrations remained constant at approximately zero throughout SCR for all three zeolites. In addition to N_2 production, H_2O and NH_4NO_3 were also produced during reactions between NO_2 and NH_3. The water produced was entirely in the gas phase over both nanocrystalline samples, but water was in the gas phase and on the surface post-SCR over Aldrich NaY. Ammonium nitrate remained condensed on the IR cell windows for all three zeolites, and therefore did not contribute to the formation of undesired gas phase products such as N_2O, NH_3 and HNO_3 that could be produced through thermal decomposition.

4.2. Nanocrystalline CuY: cationic interactions

To understand the enhancement resulting from the copper cation exchange it is necessary to consider how the nitrate and ammonia interacts with cationic reactive sites of nanocrystalline CuY. The nature of nitrate interactions with metals was studied by Gatehouse et al. using IR spectroscopy [28]. The results showed that an ionic interaction between the NO_3^- ion and a metal cation could be distinguished from a coordinated nitrate complex based on the frequencies of the vibrational modes. The adsorption of NO_2 on nanocrystalline CuY resulted in three absorbance bands due to nitrate adsorption on copper sites (Fig. 2). The central band at 1390 cm^{-1} was assigned to the ν_3 mode of the NO_3^- ion in an ionic interaction with copper cations. Ionic interactions involving nitrate likely resulted from NO_3^- formed through the sequence in reactions (1) and (2). The bands at 1313 and 1498 cm^{-1} resulted from the covalent interaction of nitrate bonded to copper through one oxygen atom and were assigned to the symmetric and asymmetric stretches (ν_1 and ν_4) of ONO_2, respectively. Nitrate adsorption could have resulted from NO_2 adsorption on Cu–O and/or EFAL sites through surface oxygen, according to reaction (3). Such adsorption is supported by the absence of a NO^+ band and seen as the shoulder to the left of the band at 1498 cm^{-1}. Comparatively, nitrate adsorption on sodium cationic sites for both NaY samples was the result of only ionic interactions. Thus, copper cation exchange introduced new sites for sorption and reaction of NO_2 in nanocrystalline CuY.

As previously mentioned, ammonia adsorption in nanocrystalline CuY resulted in two intense peaks due to the formation of $[Cu(NH_3)_4]^{2+}$. According to Flentge et al. NH_3 bonds in a square planar geometry in this complex and always in a 4:1 ratio for NH_3:Cu [34]. It is likely the majority of the copper cations were initially in sodalite cages and migrated into the supercages upon coordination with ammonia molecules [6–8,34].

Based on what has been discussed so far, an overall SCR reaction can be proposed that involves the exchanged copper cations in nanocrystalline CuY:

$$2Cu(NO_3)_2 + [Cu(NH_3)_4]^{2+} \rightarrow 4N_2 + 6H_2O + 2O_2 + Cu^{2+} + 2CuO \quad (11)$$

This reaction suggests four ammonia molecules coordinated on a copper cationic site reacted with nitrate ionically or covalently associated with copper cationic and copper–oxygen sites. A minor pathway could also involve cationic EFAL sites in place of the copper–oxygen sites. Such a reaction would produce N_2, H_2O and O_2, and Cu^{2+} and Cu–O would be restored. This is in agreement with the results, noting that N_2 and O_2 cannot be detected using IR spectroscopy.

4.3. Temperature dependence

NH_3-SCR of NO_2 was carried out at 298, 373, 423, and 473 K over all three zeolites. The reaction temperature affected the rate of reaction (discussed earlier) and, in some instances, the formation/reduction of gas phase and surface species. The amount of gas phase NO remaining post-SCR decreased with increased temperature. Gas phase NO was reduced by ~30–40% at 298 K for all zeolite samples, but reduction climbed to greater than 50%, 50% and 60% at 473 K for Aldrich NaY, nanocrystalline NaY and nanocrystalline CuY, respectively. Interestingly, NO reduction over nanocrystalline CuY was maximized to over 75% at 423 K.

At elevated reaction temperatures the amount of gas phase N_2O initially decreased as seen at 298 K, then began increasing after a few minutes of reaction. This was accompanied by a decrease in the intensity of the NH_4NO_3 bands and an increase in the intensity of gas phase and surface H_2O bands observed post-SCR. These results indicate that ammonium nitrate began thermally decomposing at the higher temperatures according to reaction (7). The amount of surface NO_3^- remaining post-SCR was reduced as reaction temperature increased, and adsorbed water increased on the zeolites post-SCR. This suggests that higher temperatures might result in a greater overall NO_x reduction, but also lead to an increase in N_2O formation.

5. Conclusions

Compared with Aldrich NaY of larger particle size, both nanocrystalline zeolites NaY and CuY showed an increased adsorption capacity for both NO_2 and NH_3. The reactive sites involved in the formation of surface species from NO_2 and NH_3 adsorption were distinct on all zeolite samples. Specifically, EFAL sites in nanocrystalline NaY and copper cationic sites in nanocrystalline CuY were responsible for the unique adsorption of reactants. Nanocrystalline NaY resulted in a 29% faster initial reaction rate for loss of gas phase NO_2 compared with commercial NaY. This was understood by the enhanced nitrate adsorption capacity, increased external surface area and increased concentration of surface reactive sites in nanocrystalline NaY. Nanocrystalline CuY resulted in a faster initial reaction rate for loss of gas phase NO_2 of 40% compared with Aldrich NaY and 11% compared with nanocrystalline NaY. This is understood as a result of copper cation exchange that increased nitrate adsorption capacity. Additionally, ammonia was activated for SCR by coordination with copper cations. An ammonium nitrate intermediate was formed in the reaction and produced gas phase N_2, O_2 and H_2O. Temperature studies showed reaction rates were independent of temperature for both Aldrich and nanocrystalline NaY, while

reaction rates for nanocrystalline CuY were inversely related to temperature.

Nanocrystalline CuY zeolite has potential as a catalyst for enhanced NO_x emission reduction through NH_3-SCR. The data presented from this work showed nanocrystalline CuY resulted in increased reaction rates for NO_2 loss at a low temperature and achieved the highest NO reduction at increased temperatures. Further studies will aim to optimize the performance of nanocrystalline CuY for deNO_x applications by identifying the most advantageous reaction temperature to maximize total NO_x reduction while maintaining faster reaction rates and by investigating the effects of oxygen and water on the rate and selectivity in NH_3-SCR.

Acknowledgements

This material is based on work supported by the Department of Energy (DE-FG-06NT42739) and the National Science Foundation (CRIF CHE-0639096).

References

[1] M. Li, Y. Yeom, E. Weitz, W.M.H. Sachtler, J. Catal. 235 (2005) 201.
[2] H. Chen, Q. Sun, B. Wen, Y. Yeom, E. Weitz, W.M.H. Sachtler, Catal. Today 96 (2004) 1.
[3] W. Song, G. Li, V.H. Grassian, S.C. Larsen, Environ. Sci. Technol. 39 (2005) 1214.
[4] Y. Li, J.N. Armor, Appl. Catal. B 1 (1992) L21.
[5] M. Iwamoto, H. Yahiro, T. Kutsuno, S. Bunyu, S. Kagawa, Bull. Chem. Soc. Jpn. 62 (1989) 583.
[6] T. Seiyama, T. Arakawa, T. Matsuda, N. Yamazoe, Y. Takita, Chem. Lett. (1975) 781.
[7] M. Iwamoto, K. Maruyama, N. Yamazoe, T. Selyama, J. Phys. Chem. 81 (7) (1977) 622.
[8] D.J. Parillo, J.P. Fortney, R.J. Gorte, J. Catal. 153 (1995) 190.
[9] J. Valyon, W.K. Hall, J. Phys. Chem. 97 (1993) 1204.
[10] J. Howard, J.M. Nicol, J. Chem. Soc. 85 (6) (1989) 1233.
[11] B. Wichterlova, Z. Sobalik, M. Skokanek, Appl. Catal. A 103 (1993) 269.
[12] G. Delahay, S. Kieger, N. Tanchoux, P. Trens, B. Coq, Appl. Catal. B 52 (2004) 251.
[13] G. Li, S.C. Larsen, V.H. Grassian, Catal. Lett. 103 (2005) 23.
[14] G. Li, S.C. Larsen, V.H. Grassian, J. Mol. Catal. 227 (2005) 25.
[15] G. Li, C.A. Jones, V.H. Grassian, S.C. Larsen, J. Catal. 234 (2005) 401.
[16] G. Madia, M. Koebel, M. Elsener, A. Wokaun, Ind. Eng. Chem. Res. 41 (16) (2002) 4008.
[17] J. Szanyi, J.H. Kwak, C.H.F. Peden, J. Phys. Chem. B 108 (2004) 3746.
[18] J. Szanyi, J.H. Kwak, R.A. Moline, C.H.F. Peden, Phys. Chem. Chem. Phys. 5 (2005) 4045.
[19] J.H. Kwak, C.H.F. Peden, J. Szanyi, Catal. Lett. 109 (2006) 1.
[20] Y.H. Yeom, J. Henao, M.J. Li, W.M.H. Sachtler, E. Weitz, J. Catal. 231 (2005) 181.
[21] Y.H. Yeom, B. Wen, W.M.H. Sachtler, E. Weitz, J. Phys. Chem. B 108 (2004) 5386.
[22] F. Gilles, J.L. Blin, H. Toufar, M. Briend, B.L. Su, Colloid Surf. A: Physiochem. Eng. Aspects 241 (2004) 245–252.
[23] C.A. Jones, S.C. Larsen, Catal. Lett. 78 (1–4) (2002) 243.
[24] W. Song, V.H. Grasssian, S.C. Larsen, Chem. Commun. (23) (2005) 2951.
[25] C. Sedlmair, B. Gil, K. Seshan, A. Jentys, J.A. Lercher, Phys. Chem. Chem. Phys. 5 (2003) 1897.
[26] P.J. Carl, S.C. Larsen, J. Phys. Chem. B 104 (2000) 6568.
[27] P.J. Carl, S.C. Larsen, J. Catal. 182 (1999) 208.
[28] J.C. Conesa, J. Soria, J. Magn. Res. 33 (1979) 295;
B.M. Gatehouse, S.E. Livingstone, R.S. Nyholm, J. Chem. Soc. (1957) 4222.
[29] G. Li, M. Xu, S.C. Larsen, V.H. Grassian, J. Mol. Catal. A 194 (2003) 169.
[30] M. Wallin, H. Gronbeck, A.L. Spetz, M. Skoglundh, Appl. Surf. Sci. 235 (2004) 487.
[31] M.W. Urban, Vibrational Spectroscopy of Molecules and Macromolecules on Surfaces, John Wiley & Sons Inc., 1993.
[32] H. Kosslick, H. Berndt, H.D. Lanh, A. Martin, H. Miessner, V.A. Tuan, J. Chem. Soc. Faraday Trans. 90 (18) (1994) 2837.
[33] M. Niwa, S. Nishikawa, N. Katada, Micropor. Mesopor. Mater. 82 (2005) 105.
[34] D.R. Flentge, J.H. Lunsford, P.A. Jacobs, J.B. Uytterhoeven, J. Phys. Chem. 79 (1975) 354.